

# Nanoscale

Accepted Manuscript



This is an *Accepted Manuscript*, which has been through the Royal Society of Chemistry peer review process and has been accepted for publication.

*Accepted Manuscripts* are published online shortly after acceptance, before technical editing, formatting and proof reading. Using this free service, authors can make their results available to the community, in citable form, before we publish the edited article. We will replace this *Accepted Manuscript* with the edited and formatted *Advance Article* as soon as it is available.

You can find more information about *Accepted Manuscripts* in the [Information for Authors](#).

Please note that technical editing may introduce minor changes to the text and/or graphics, which may alter content. The journal's standard [Terms & Conditions](#) and the [Ethical guidelines](#) still apply. In no event shall the Royal Society of Chemistry be held responsible for any errors or omissions in this *Accepted Manuscript* or any consequences arising from the use of any information it contains.

## ARTICLE

# Facile fabrication of a near-infrared responsive nanocarrier for spatiotemporally controlled chemo-photothermal synergistic cancer therapy

Cite this: DOI: 10.1039/x0xx00000x

Hao Wan,<sup>ab</sup> Yi Zhang,<sup>a</sup> Zheyi Liu,<sup>a</sup> Guiju Xu,<sup>a</sup> Guang Huang,<sup>a</sup> Yongsheng Ji,<sup>a</sup> Zhichao Xiong,<sup>ab</sup> Quanqing Zhang,<sup>a</sup> Jing Dong,<sup>a</sup> Weibing Zhang<sup>\*b</sup> and Hanfa Zou<sup>\*a</sup>

Received 00th January 2012,

Accepted 00th January 2012

DOI: 10.1039/x0xx00000x

[www.rsc.org/](http://www.rsc.org/)

Remote controlled nanocarriers for drug delivery are of great promise to provide in time, sensitive and spatiotemporally selective treatments in cancer therapy. Due to the convenient and precise manipulation, deep penetration through tissues and excellent biocompatibility, near-infrared (NIR) irradiation is a preferentially external stimulus in triggering the release of loaded drugs. In this work, a NIR responsive nanocarrier was fabricated based on the decoration of the reduced graphene oxide nanosheets (rNGO) with the mesoporous silica shell and subsequent functionalization of the thermoresponsive polymer brushes (pNIPAM-co-pAAm) onto the outlet of the silica pore channels for spatiotemporally controlled chemo-photothermal synergistic cancer therapy. rNGO, which combined with the mesoporous silica shell to provide the high loading capacity of anticancer drug (doxorubicin, DOX), were assigned to sense NIR irradiation for the manipulation of the pNIPAM-co-pAAm valve to control the diffusion of loaded DOX. Under NIR irradiation, rNGO would generate heats, which could not only elevate the surrounding temperature over the low critical solution temperature (LCST) of pNIPAM-co-pAAm to open the thermoresponsive polymer valve and promote the diffusion of DOX, but also serve as the photothermal therapy during the treatments. By manipulating NIR irradiation, the nanocarrier exhibited efficiently controlled release of loaded DOX both in the buffer and in living HeLa cells (the model cancer cells), providing powerful and site-targeted treatments attributed to synergistic effects of chemo-photothermal therapy. To sum up, this novel nanocarrier presents to be an excellent drug delivery platform in remote controlled chemo-photothermal synergistic cancer therapy via NIR irradiation.

## Introduction

Controlled release of the loaded drugs from the nanocarriers guarantees relatively stable therapeutic efficacy during the treatments, which is preferred in cancer therapy.<sup>1-3</sup> Remote controlled nanocarriers, due to the convenient, sensitive, precise and long-range manipulation of drug release according to the external stimuli (magnetic,<sup>4</sup> electric fields,<sup>5</sup> and ultrasound,<sup>6</sup> etc.), have been receiving more and more attentions in recent years. Compared with other remote stimuli, light irradiation could be targeted at the specific tumour tissues and activated at the desired time point, leaving minimal side effects for normal tissues. Ultraviolet or visible (UV or Vis) irradiation has already been utilized in remote controlled drug release,<sup>7-10</sup> yet which suffers from the potential phototoxicity for normal cells and limited tissue penetration, restricting the practical applications. Near-infrared (NIR) light (wavelength between 750 and 1000 nm), capable of deeply penetrating into human tissues with high biocompatibility and lower scattering property, has been demonstrated as a promising stimulus in the remote controlled drug release. Various drug delivery systems (DDS), including inorganic particles,<sup>11</sup> polymer micelles,<sup>12, 13</sup> liposomes,<sup>14, 15</sup> metal complexes,<sup>16</sup> etc., have already been synthesized as NIR controlled nanocarriers for cancer chemotherapy.

Meanwhile, NIR irradiation has also been widely utilized for photothermal therapy as an external stimulus owing to the NIR-adsorbing ability of plasmonic materials (gold nanorod,<sup>17</sup> CuS,<sup>18</sup> Cu<sub>2</sub>Se,<sup>19</sup> etc.), which could convert the adsorbed photon energy into heats efficiently.<sup>20</sup> As an efficient and minimally invasive strategy to deal with cancer issues, photothermal therapy induces cell death via the hyperthermia effect. The synergistic treatments combining both photothermal therapy and chemotherapy have emerged as a novel choice to exploit each other's merits for presenting powerful treatments during cancer therapy,<sup>16, 21-23</sup> which therefore make the preparation of a NIR controlled nanocarrier with chemo-photothermal synergistic therapy promising.

The reduced graphene oxide (rGO) has been applied in various fields owing to its unique chemical and physical properties.<sup>24-26</sup> As a commonly used photothermal agent,<sup>27-29</sup> excellent stability, low cost, negligible toxicity, high surface area and large-scale production make the rGO attractive and imply great potentials in biological applications.<sup>30-32</sup> However, poor dispersibility in the physiological condition as well as difficult modification hinder the further intracellular utilization of rGO.

The coating of rGO with an outer shell exhibited a strategy to enhance the dispersibility as well as the possibility for the modification of rGO,<sup>33-35</sup> among which the mesoporous silica has attracted attentions, owing to excellent biocompatibility, high

surface area, easy synthesis and modification.<sup>36</sup> The mesoporous silica shell coated rGO (rGO@mSiO<sub>2</sub>) has already been utilized for selective enrichment of endogenous peptides,<sup>37</sup> energy storage,<sup>38</sup> templated fabrication of sandwich-like mesoporous carbon and metal oxide materials.<sup>39</sup> But the application of rGO@mSiO<sub>2</sub> in intracellular drug delivery is still in its infancy.<sup>40</sup> Specifically, it is easily assumed that the combination of rGO and the mesoporous silica shell would make the rGO@mSiO<sub>2</sub> suitable as a novel nanocarrier. At first, the vertical pore channels of the mesoporous silica shell and the  $\pi$ - $\pi$  stacking between rGO and some aromatic anti-cancer drugs would contribute to the high loading capacity; Secondly, the coating of rGO with the mesoporous silica shell not only enhance the dispersibility in the physiological condition but also the ability for further modification; Finally, the involvement of rGO would provide the nanocarrier with photothermal ability to improve the treating efficacy. However, the pristine rGO@mSiO<sub>2</sub> with loaded drugs might suffer from the pre-leakage of drugs, which would cause severe damages for normal cells during treatments. Thus, a stimuli-responsive valve combined with the rGO@mSiO<sub>2</sub> would better fulfil controlled drug delivery for cancer therapy, making the administration for cancer cells “on-demand”.

pNIPAM, a thermoresponsive polymer, would transform between hydrophilic and hydrophobic states according to the change of environment temperature.<sup>41, 42</sup> Because of this special property and negligible toxicity, the pNIPAM has been used as the thermoresponsive polymer valve outside the pore channels of various materials, including mesoporous silica nanoparticles<sup>43</sup> and ordered porous anodic aluminum oxide,<sup>44</sup> etc., to control the release of loaded agents in the water-based environment. When the surrounding temperature is below LCST, the polymer brushes of pNIPAM would become hydrophilic and stretched out, which could hinder the diffusion of loaded agents. However, when the external temperature exceeds the LCST, the polymer brushes would become hydrophobic and collapsed to open the pore channels for the release of loaded agents. Diverse external stimuli, such as temperature,<sup>45, 46</sup> UV irradiation<sup>9</sup> and salts,<sup>47</sup> have been applied to control the “open-closed” transition of this thermoresponsive polymer valve straightforward or indirectly, yet where few have been reported to be controlled by NIR irradiation to the best of our knowledge.<sup>48, 49</sup>

Herein, to prepare a stable and low toxicity nanocarrier for spatiotemporally NIR controlled chemo-photothermal synergistic cancer therapy, we elaborately fabricated a novel nanocarrier composed of the mesoporous silica shell with a thermoresponsive polymer valve functionalized reduced graphene oxide nanosheets (rNGO@mSiO<sub>2</sub>@pNIPAM-co-pAAm), which was used for the intracellular delivery of the anticancer drug DOX in living HeLa cells. Without NIR irradiation, the thermoresponsive polymer valve stayed hydrophilic to close the silica pore channels, efficiently reducing the undesired pre-leakage of DOX during the incubation. Under the exposure of NIR irradiation, heats generated by rNGO would elevate the surrounding temperature over the LCST of pNIPAM-co-pAAm to open the silica pore channels and promote the release of DOX as well as provide photothermal administration for cancer cells. The as-synthesized nanocarrier demonstrated to be low toxicity with good dispersibility, stability and high loading capacity of DOX. The release of loaded DOX was successfully manipulated by the thermoresponsive polymer valve via NIR irradiation, and the involvement of rNGO also exhibited effective treatments for HeLa cells via the photothermal administration. Finally, the chemo-photothermal synergistic treatments with DOX loaded rNGO@mSiO<sub>2</sub>@pNIPAM-co-pAAm exhibited site-targeted and highly efficient therapy for HeLa cells under the stimulus of NIR irradiation.

## Experimental section

### Materials

Hexadecyltrimethyl ammonium bromide (CTAB), tetraethyl orthosilicate (TEOS, 99%), N-isopropylacrylamide (NIPAM, 97%), acrylamide (AAm, 99%), CuBr, pentamethyldiethylenetriamine (PMDETA, 99%), (3-aminopropyl)triethoxysilane (APTEOS, 99%), Trypan blue were purchased from Sigma-Aldrich (St. Louis, MO, USA). RPMI 1640 medium was obtained from Invitrogen (Carlsbad, CA). Ammonium nitrate, sodium hydroxide, triethylamine, isopropanol and ethanol were obtained from Tianjin Kermel plant of chemical reagent (Tianjin, China). 2-bromoisobutyryl bromide and doxorubicin in the form of hydrochloride salt were purchased from Aladdin Corporation (Shanghai, China). Deionized water used for all experiments was purified with a Milli-Q water system.

### Preparation of the mesoporous silica shell coated reduced graphene oxide nanosheets (rNGO@mSiO<sub>2</sub>)

Graphene oxide sheets obtained through modified Hummers' method were sonicated for 3 h at 600 W and centrifuged at 22000 g for another 3 h to remove large-sized graphene oxide sheets and get nano-sized graphene oxide sheets (NGO). The 10 mg obtained NGO were redispersed in 18 mL NaOH solution (pH=12.0) and magnetically stirred overnight at 80 °C for the mild reduction (rNGO). Then, 372 mg CTAB was added into this mixture whose pH was adjusted to 11.8 by 2 M NaOH. After the mixture was stirred for 0.5 h, 200  $\mu$ L TEOS was added and kept stirring for another 24 h. The resulting product was collected by centrifugation and washed with deionized water and ethanol.

### Grafting of thermoresponsive pNIPAM-co-pAAm brushes onto rNGO@mSiO<sub>2</sub> via surface-initiated atom transfer radical polymerization (rNGO@mSiO<sub>2</sub>@pNIPAM-co-pAAm)

To immobilize initiator onto the rNGO@mSiO<sub>2</sub>, APTEOS (1 mL) was added dropwise to the isopropanol solution of rNGO@mSiO<sub>2</sub> (30 mg). After the solution was magnetically stirred for 24 h at room temperature, the amine-modified rNGO@mSiO<sub>2</sub> (rNGO@mSiO<sub>2</sub>-NH<sub>2</sub>) was isolated, followed by washed with 50 mL isopropanol and 50 mL dichloromethane for three times, and redispersed in 50 mL anhydrous dichloromethane. As soon as the addition of distilled triethylamine (0.595 mL), the whole solution was put in an ice bath under argon atmosphere. After the solution was cooled to 0 °C, 2-bromoisobutyryl bromide (0.528 mL) was added dropwise. The resulting solution was magnetically stirred for 2 h at 0 °C and then warmed up to room temperature for another 16 h reaction (rNGO@mSiO<sub>2</sub>-Br). The surfactant occupied in the silica pore channels was extracted by 120 mL solution of 80 mg NH<sub>4</sub>NO<sub>3</sub> in 95% ethanol at 70 °C for 1 h.

To graft thermoresponsive pNIPAM-co-pAAm brushes onto the outlet of rNGO@mSiO<sub>2</sub>, 10 mg above rNGO@mSiO<sub>2</sub>-Br, 1.80 g NIPAM and 0.18 g AAm were dispersed in a mixture of 5 mL H<sub>2</sub>O and 5 mL methanol in a Schlenk flask, followed by three pump-thaw-refill cycles (Schlenk line). While the mixture was frozen, CuBr (0.010 g) and PMDETA (35  $\mu$ L) were added. The frozen mixture was left to melt at room temperature, followed by 6 h magnetical stir. The polymerization was terminated by exposing to air and pouring water into the Schlenk tube.

### Temperature controlled release of the loaded DOX

For the loading process, each centrifugation tube containing 0.3 mg DOX (in 20  $\mu$ L DMSO), 0.1 mg rNGO@mSiO<sub>2</sub>@pNIPAM-co-

pAAm or equivalent amount of rNGO@mSiO<sub>2</sub> and 1 mL PBS buffer (pH=7.4) were shaken for 24 h at 45 °C in the dark. After that, the tubes were placed in 0 °C for 10 min and the material was washed by cool PBS buffer twice to remove the DOX adsorbed on the outlet of rNGO@mSiO<sub>2</sub>@pNIPAM-co-pAAm or rNGO@mSiO<sub>2</sub>. Finally, the tubes were centrifuged at 20000 g for 5 min to collect the precipitation.

For temperature controlled release, the above precipitation divided into two groups was put in 50 °C and 37 °C, respectively and started the release process by adding 1.5 mL KH<sub>2</sub>PO<sub>4</sub> (pH=5) or PBS (pH=7.4) buffer into each tube under the gentle vibration. At a given time, one tube was taken out to be placed in cold water for 5 min and centrifuged at 20000 g to collect the supernatant to determine the release amount by UV-Vis analysis.

### Effect of laser-induced the change of temperature

Various concentrations of rNGO@mSiO<sub>2</sub>@pNIPAM-co-pAAm were dispersed in the PBS buffer and irradiated by 3 W or 6 W NIR laser at the wavelength of 808 nm for 500 s. Every 100 s the temperature was recorded using a digital thermometer. The control experiment of negative sample (only the PBS buffer) was also measured under the same condition.

### NIR controlled release of the loaded DOX

For the loading process, 3 mg rNGO@mSiO<sub>2</sub>@pNIPAM-co-pAAm or equivalent amount of rNGO@mSiO<sub>2</sub> in 30 mL PBS buffer (pH=7.4) was mixed with a solution of 9 mg DOX in 1 mL DMSO at 45 °C for 24 h in the dark. After that, the DOX loaded rNGO@mSiO<sub>2</sub>@pNIPAM-co-pAAm or rNGO@mSiO<sub>2</sub> was placed in 0 °C for 10 min and washed by 15 mL cool PBS buffer twice to remove the DOX adsorbed on the outlet of the rNGO@mSiO<sub>2</sub> or rNGO@mSiO<sub>2</sub>@pNIPAM-co-pAAm as well as close the thermoresponsive polymer valve.

For NIR controlled release, the above DOX loaded rNGO@mSiO<sub>2</sub>@pNIPAM-co-pAAm or rNGO@mSiO<sub>2</sub> was dispersed in 10 mL KH<sub>2</sub>PO<sub>4</sub> (pH=5) buffer at 37 °C. At determined time, the mixture was irradiated by NIR (6 W) and 0.1 mL mixture was taken out before and after irradiation for the UV-Vis measurement.

### The simulative in vivo heating and drug release behaviour under NIR irradiation

The centrifugation tube containing KH<sub>2</sub>PO<sub>4</sub> solution (pH=5) of DOX loaded rNGO@mSiO<sub>2</sub>@pNIPAM-co-pAAm was encompassed by different thickness (1.5, 3 and 5 mm) of fresh meat and irradiated by NIR for 300 s. Every 60 s the temperature was recorded using a digital thermometer. The drug release behaviour was recorded in the case of 3 mm thickness meat. The release amount of DOX with or without 10 min NIR irradiation was determined by the UV-Vis measurement.

### In vitro cytotoxicity assay

HeLa cells were seeded in a 96-well plate at the number of 3\*10<sup>3</sup> per well with 100 µL media. After the cells were incubated in a humidified atmosphere of 5% CO<sub>2</sub> at 37 °C for 12 h, a series of rNGO@mSiO<sub>2</sub>@pNIPAM-co-pAAm with different concentrations were added. After incubation for 24, 48 and 72 h, respectively, the cell viability was determined by cell-counting kit-8 (CCK-8) assay.

For NIR controlled chemo-photothermal synergistic therapy, before adding anything, the HeLa cells at the number of 3\*10<sup>3</sup> per well were incubated for 24 h. The bare rNGO@mSiO<sub>2</sub>@pNIPAM-

co-pAAm, DOX loaded rNGO@mSiO<sub>2</sub> or rNGO@mSiO<sub>2</sub>@pNIPAM-co-pAAm was added at determined concentration equivalent to the amount of free DOX. After incubation for 4 h, each well was washed by the PBS buffer twice to remove the DOX, rNGO@mSiO<sub>2</sub> and rNGO@mSiO<sub>2</sub>@pNIPAM-co-pAAm not uptaken by cells. Every line of wells was irradiated by NIR for 10 min at the laser power of 6 W for NIR-irradiated group (rNGO@mSiO<sub>2</sub>@pNIPAM-co-pAAm/NIR, rNGO@mSiO<sub>2</sub>@pNIPAM-co-pAAm/DOX/NIR) and the other incubation conditions were the same for non-NIR-irradiated group (free DOX, rNGO@mSiO<sub>2</sub>/DOX and rNGO@mSiO<sub>2</sub>@pNIPAM-co-pAAm/DOX). After incubation for another 8 h, the cell viability was measured by cell-counting kit-8 (CCK-8) assay.

### Confocal laser scanning microscopy imaging experiment

The HeLa cells were seeded at a number of 5\*10<sup>4</sup> per well as two groups and incubated for another 48 h. After that, the rNGO@mSiO<sub>2</sub>@pNIPAM-co-pAAm at the concentration of 60 µg/mL containing 12 µg/mL DOX was added to each group and interacted with the cells for 4 h, followed by twice wash with the PBS buffer and incubation for another 2 h with or without 10 min NIR irradiation. Finally, the images of cells were taken under the confocal laser scanning microscope.

### Survival states of HeLa cells under optical microscope imaging

For visual identification of the survival states of HeLa cells after different treatments, experimental groups were stained with 0.4% Trypan blue for 5 min after different incubation conditions (rNGO@mSiO<sub>2</sub>@pNIPAM-co-pAAm/DOX, rNGO@mSiO<sub>2</sub>@pNIPAM-co-pAAm/NIR, rNGO@mSiO<sub>2</sub>/DOX, rNGO@mSiO<sub>2</sub>@pNIPAM-co-pAAm/DOX/NIR), followed by twice wash with the PBS buffer. The images of cells were then taken under an optical microscope.

The site-targeted NIR controlled cancer therapy ability was conducted through employing 60 µg/mL rGO@mSiO<sub>2</sub>@pNIPAM-co-pAAm containing 12 µg/mL DOX to treat with HeLa cells in the culture plate for 12 h, where only one part of region was exposed under 10 min NIR irradiation. The optical images of HeLa cells were taken after stain with Trypan blue.

### Characterization

Transmission electron microscopy (TEM) was conducted on a JEOL 2000 EX electronic microscope with an accelerating voltage of 120 keV. Fourier transformed infrared spectroscopy (FTIR) characterization has been performed on Thermo Nicolet 380 spectrometer using KBr pellets (Nicolet, Wisconsin, USA). The nitrogen adsorption measurement of rNGO@mSiO<sub>2</sub> was conducted at -196 °C (liquid nitrogen temperature) using a static-volumetric method on ASAP 2010 (Micromeritics, USA). Pore diameter and distribution curves were calculated by BJH (Barrett-Joyner-Halenda) method from adsorption branch. The Raman spectra were obtained on a Via-Reflex with excitation from an argon ion laser (532 nm). Thermogravimetry (TGA) was performed in a Perkin-Elmer Pyris Diamond TG/DTA analyser, with 10 °C /min heating ramps, from room temperature to 800 °C. UV-Vis spectra were recorded on a UV-3101PC Shimadzu spectroscope. The confocal laser scanning microscopy (CLSM) imaging was performed by a FluoViewTM FV1000 confocal laser scanning microscope (Olympus, Japan) with an 100\*objective. The cells were pre-planted in the glass-bottom dishes (NEST, China). The optical images were taken under Olympus CKX 41 microscope (Olympus, Japan). The EDS element

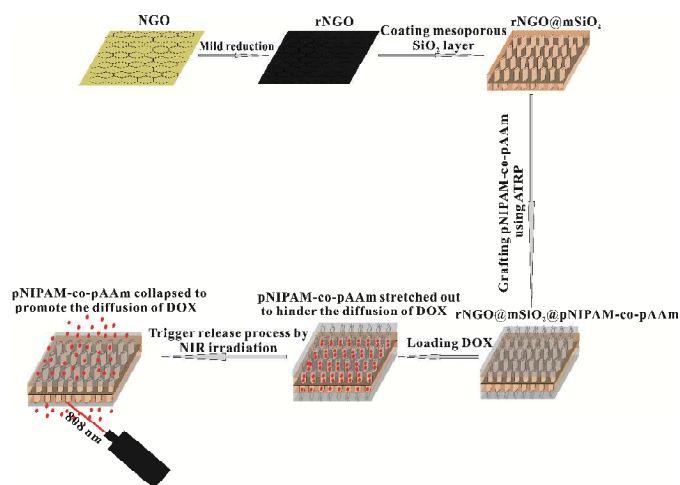


**Fig. 1** The schematic illustration of the fabrication process of rNGO@mSiO<sub>2</sub>@pNIPAM-co-pAAm.

mapping was conducted on the Inca X-Max80 EDS system (Oxford, England).

## Results and discussion

### Fabrication and characterization of rNGO@mSiO<sub>2</sub>@pNIPAM-co-pAAm

The process for the fabrication of rNGO@mSiO<sub>2</sub>@pNIPAM-co-pAAm is illustrated in Fig. 1. At first, the graphene oxide nanosheets (NGO) with a lateral size around 200-300 nm were synthesized based on a modified Hummer's method coupled with repeated ultrasonication and centrifugation. Then, the obtained NGO were mildly reduced (rNGO) by NaOH at 80 °C with the brown solution turning into black solution (Fig. S1†).<sup>35</sup> Via the hydrolysis of TEOS solution containing CTAB, the mesoporous silica shell of about 30 nm thickness with vertical pore channels was assembled onto the rNGO to obtain a sandwich-like structure (Fig. 2b, 2c and S2a†).<sup>2a</sup> Finally, the rNGO@mSiO<sub>2</sub> immobilized with the bromoisobutryl bromide as the initiator was utilized to trigger the polymerization of NIPAM and AAm with the atom transfer radical polymerization (ATRP) strategy. Unlike regular radical polymerization, ATRP was a controlled polymeric method which would generate homogenous polymer brushes beneficial for the controlled release of loaded drugs. According to previous studies, the LCST of pNIPAM was affected mostly by the composition ratio of the hydrophilic and hydrophobic components in the polymer brushes, where basically higher LCST would be achieved with more hydrophilic components.<sup>36</sup> In consideration that the incubation temperature for HeLa cells was 37 °C, the composition ratio between NIPAM and hydrophilic AAm was optimized to make the LCST at 41 °C as indicated by the transparent solution turning cloudy based on a previous study.<sup>50</sup> In this condition, the polymer brushes would stay hydrophilic and stretched out during incubation to hinder the pre-leakage of loaded drugs (Table S3†). The successful grafting of pNIPAM-co-pAAm polymer brushes was confirmed by the appearance of a polymer corona around rNGO@mSiO<sub>2</sub> shown in the TEM images (Fig. 2d, S2b† and S2c†).<sup>40</sup> The characterization of the newly synthesized rNGO@mSiO<sub>2</sub>@pNIPAM-co-pAAm was carefully investigated. Pristine NGO exhibited poor ability in NIR adsorption, and therefore the mild reduction of NGO was carried out to recover the sp<sup>2</sup> structure for enhancing the efficiency of converting NIR irradiation

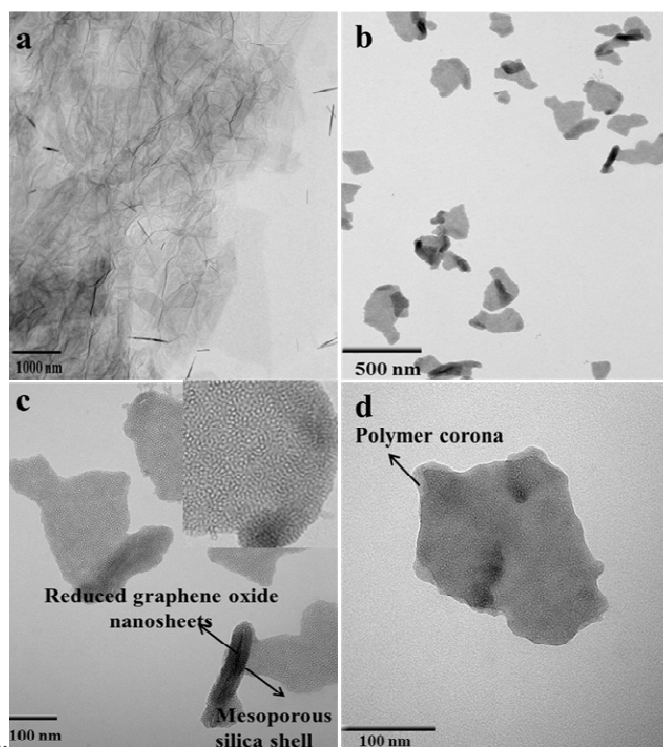


**Fig. 2** TEM images of GO (a); rNGO@mSiO<sub>2</sub> (b, c); rNGO@mSiO<sub>2</sub>@pNIPAM-co-pAAm (d).

into heats.<sup>51</sup> The UV-Vis-NIR spectrometry analysis showed a negligible adsorption by NGO in the NIR region of 750 nm-1000 nm, while after mild reduction by NaOH at 80 °C for 12 h, an intense adsorption by rNGO in the NIR range could be observed (Fig. 3a). Besides, the Raman spectrum of rNGO@mSiO<sub>2</sub>@pNIPAM-co-pAAm showed two broad overlapping bands at around 1320 cm<sup>-1</sup> (D-mode) and 1587 cm<sup>-1</sup> (G-mode), further illustrating the existence of rNGO (Fig. S4†). After the rNGO were coated with the mesoporous silica shell, the nitrogen adsorption-desorption isotherm of rNGO@mSiO<sub>2</sub> showed the typical IV isotherm pattern of the mesoporous material and a characteristic adsorption step in the 0.1–0.3 relative pressure range, which hinted that the material possessed a narrow distribution of pore size (Fig. 3b). The small-angle XRD pattern showed that rNGO@mSiO<sub>2</sub> had a hexagonally ordered structure (Fig. S5a†). According to the results of Brunauer-Emmett-Teller analysis, the composite material exhibited a high surface area (1067 m<sup>2</sup>/g) and a large pore volume (1.10 g/cm<sup>3</sup>) with the pore diameter at 3.28 nm (Fig. S5b†), implying potential high loading capacity of DOX in the rNGO@mSiO<sub>2</sub>@pNIPAM-co-pAAm. The rNGO@mSiO<sub>2</sub> was immobilized with bromoisobutryl bromide for the initiation of the following polymerization, which was characterized with FTIR analysis (Fig. 3c). The peak at 1084 cm<sup>-1</sup> corresponding to –Si-O-Si– demonstrated the assembly of the mesoporous silica shell (Fig. 3c1) and peaks of amide bands at 1650 cm<sup>-1</sup> (C=O stretching) and 1553 cm<sup>-1</sup> (N-H stretching) confirmed the involvement of the initiator (Fig. 3c2). After the ATRP reaction, the enhanced intensity of the peaks at 1650 cm<sup>-1</sup> (C=O stretching), 1553 cm<sup>-1</sup> (N-H stretching) and the emerged peaks at 2924, 2976 cm<sup>-1</sup> (sp<sup>3</sup> C-H) were observed with the rNGO@mSiO<sub>2</sub>@pNIPAM-co-pAAm, which demonstrated the successful grafting of polymer brushes (Fig. 3c3). According to the EDS element mapping results, all the fundamental elements (O, Si, C, N) distributed uniformly within the nanocarrier (Fig. S6†). Finally, the TGA characterization was used to investigate the mass ratio of different compositions in

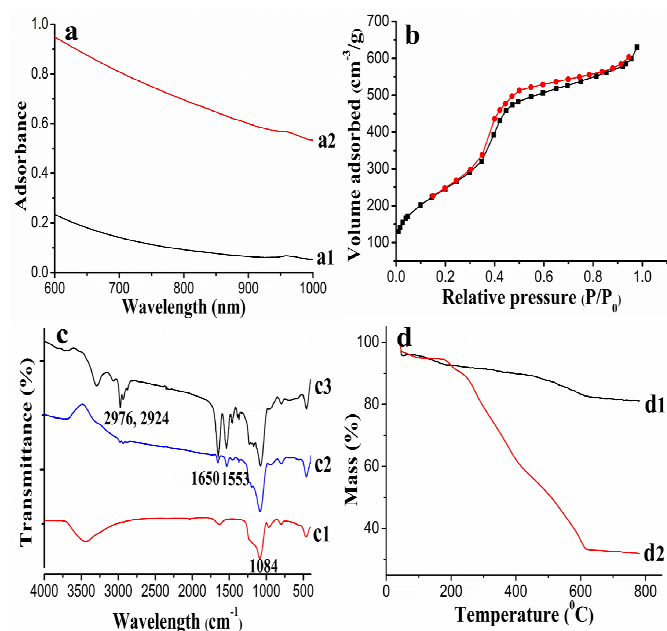


**Fig. 3** UV-Vis-NIR spectrometry analysis of rNGO (a1) and rNGO (a2); N<sub>2</sub> adsorption-desorption isotherm of rNGO@mSiO<sub>2</sub> (b); FTIR spectra of rNGO@mSiO<sub>2</sub> (c1), rNGO@mSiO<sub>2</sub>@Br (c2) and rNGO@mSiO<sub>2</sub>@pNIPAM-co-pAAm (c3); TGA spectra of rNGO@mSiO<sub>2</sub> (d1) and rNGO@mSiO<sub>2</sub>@pNIPAM-co-pAAm (d2).

the rNGO@mSiO<sub>2</sub>@pNIPAM-co-pAAm. As seen in Fig. 3d1, the rNGO weighed ca. 20% of the rNGO@mSiO<sub>2</sub>. It can be observed in Fig. 3d2 that the maximum mass loss happened around 300–600 °C, corresponding to the decomposition of pNIPAM-co-pAAm and rNGO, which implied that thermoresponsive polymer took up ca. 47% weight of the rNGO@mSiO<sub>2</sub>@pNIPAM-co-pAAm when rNGO@mSiO<sub>2</sub> was used as a reference.

### Temperature controlled release of loaded DOX from rNGO@mSiO<sub>2</sub>@pNIPAM-co-pAAm

The thermoresponsive pNIPAM-co-pAAm was assigned to block the pore channels of the mesoporous silica shell based on the states transforming of polymer brushes between hydrophilicity and hydrophobicity in response to the environment temperature. The LCST of the pNIPAM-co-pAAm was optimized at 41 °C according to a previous study,<sup>50</sup> for which the polymer brushes would form the inter-molecule hydrogen bonds with water molecules to maintain hydrophilic and stretched out to favour the storage of loaded drugs during incubation; while once the environment temperature exceeded the LCST, the polymer brushes would form intra-molecule hydrogen bonds between polymer chains to become hydrophobic and collapsed to open the silica pore channels for releasing the loaded drugs.

Then, the feasibility of the thermoresponsive polymer valve in controlling the release of DOX was evaluated under different temperatures via UV-Vis measurement at 480 nm. The loading capacity of rNGO@mSiO<sub>2</sub>@pNIPAM-co-pAAm for DOX reached 0.8221±0.12 g/g at 45 °C in 24 h attributed to the storage via both π-π stacking by rNGO and physical adsorption by silica pore channels. As shown in Fig. 4d, when the environment temperature was 37 °C (physiological condition, below the LCST), the rNGO@mSiO<sub>2</sub>@pNIPAM-co-pAAm showed a negligible release of DOX with respect to a sustainable release for the case of rNGO@mSiO<sub>2</sub> without the thermoresponsive polymer valve (Fig. 4c), in addition, when the environment temperature was elevated to

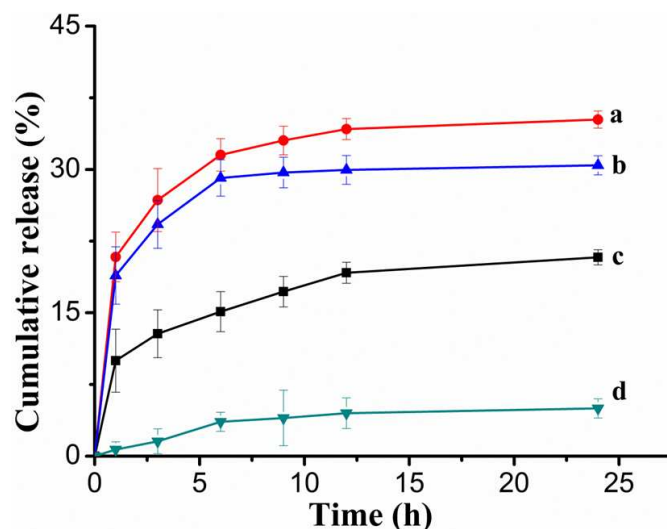


**Fig. 4** The release of loaded DOX in 24 h at 50 °C and pH=5 from rNGO@mSiO<sub>2</sub> (a) or rNGO@mSiO<sub>2</sub>@pNIPAM-co-pAAm (b); the release of loaded DOX in 24 h at 37 °C and pH=5 from rNGO@mSiO<sub>2</sub> (c) or rNGO@mSiO<sub>2</sub>@pNIPAM-co-pAAm (d).

50 °C (above the LCST), the release of DOX from rNGO@mSiO<sub>2</sub>@pNIPAM-co-pAAm and rNGO@mSiO<sub>2</sub> both showed a similarly sustainable release pattern (Fig. 4a and 4b), all of which hinted the utility of the thermoresponsive polymer valve in control of the release of DOX. Moreover, the higher temperature would promote the release of DOX due to the heats-stimulative dissociation of the strong interactions, including π-π stacking and silica pore channels adsorption (Fig. 4a and 4c). Besides, the lower pH (pH=5) mimicking the interior atmosphere of HeLa cells could promote the protonation of DOX, which would enlarge the overall amount of release beneficial for the chemotherapy as indicated in Fig. S7†.

### NIR controlled release of loaded DOX from rNGO@mSiO<sub>2</sub>@pNIPAM-co-pAAm

In the rNGO@mSiO<sub>2</sub>@pNIPAM-co-pAAm, rNGO were assigned to produce heats under NIR irradiation (808 nm) to manipulate the following DOX release, and the heating effect by the rNGO@mSiO<sub>2</sub>@pNIPAM-co-pAAm was first investigated. Shown in Fig. 5, more heats would be generated by rNGO@mSiO<sub>2</sub>@pNIPAM-co-pAAm with longer irradiation time, higher concentration and more powerful laser. So in order to completely open the pNIPAM-co-pAAm valve (T>41 °C) and maximize the chance of cell death by hyperthermia (T>42 °C),<sup>42</sup> a laser power of 6 W was chosen in the following experiments.

Since the pNIPAM-co-pAAm would transform between hydrophilicity and hydrophobicity according to the environment temperature, the rNGO@mSiO<sub>2</sub>@pNIPAM-co-pAAm could be dispersed homogeneously in the PBS buffer to form a transparent solution at 37 °C; while under the exposure of NIR irradiation for 5 min, the solution turned cloudy quickly (Fig. S8†), and the cloudy solution appeared transparent again when NIR irradiation was off. The process could be repeated for more than 10 on/off cycles without any different phenomenon, confirming the excellent stability of the reversible transformation ability of rNGO@mSiO<sub>2</sub>@pNIPAM-co-pAAm via the control of NIR irradiation.

Later, the remote controlled release of loaded DOX from rNGO@mSiO<sub>2</sub>@pNIPAM-co-pAAm through NIR irradiation was

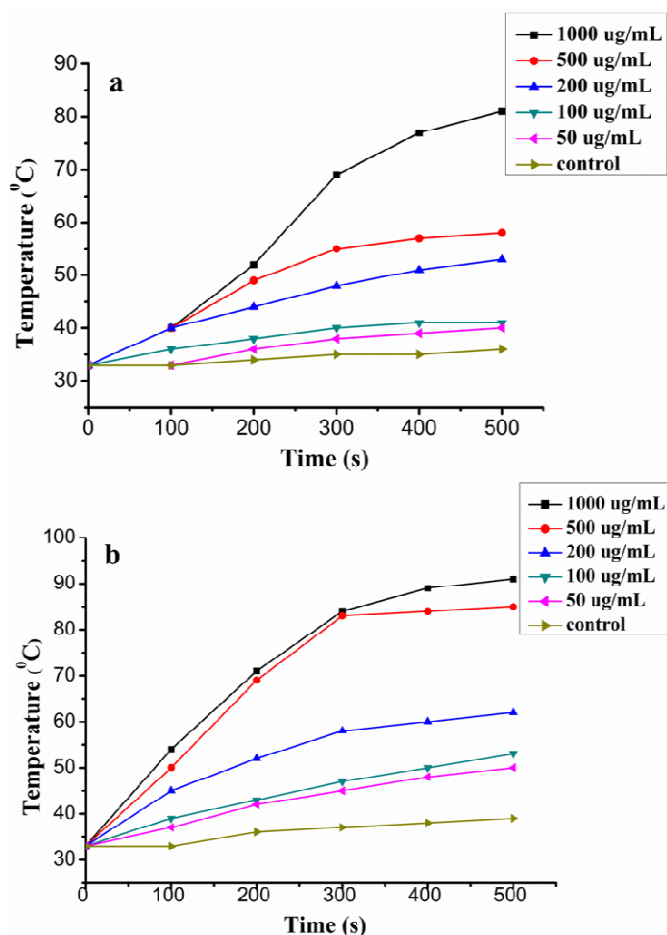


**Fig. 5** The change of temperature of rNGO@mSiO<sub>2</sub>@pNIPAM-co-pAAm solution in 500 s after exposure under NIR irradiation with the wavelength of 808 nm at the laser power of 3 W (a) or 6 W (b).

verified where the release of loaded DOX from rNGO@mSiO<sub>2</sub> was conducted as a control. Under NIR irradiation at determined time, the release amount of loaded DOX in the KH<sub>2</sub>PO<sub>4</sub> (pH=5) buffer before and after irradiation was measured. An intense increase of the released DOX was obtained in both cases after NIR irradiation. However, the release of DOX from rNGO@mSiO<sub>2</sub>@pNIPAM-co-pAAm could hardly be detected without NIR irradiation in relative to a sustainable release in the case of rNGO@mSiO<sub>2</sub> (Fig. 6a). Thus, it further demonstrated the thermoresponsive polymer valve could efficiently control the release of DOX by the manipulation of solution temperature in response to NIR irradiation.

Then, the feasibility of NIR controlled release of loaded DOX from rNGO@mSiO<sub>2</sub>@pNIPAM-co-pAAm in living HeLa cells was profiled. The confocal laser scanning microscopy (CLSM) imaging was employed to monitor the intracellular release of DOX. Shown in Fig. 6b, it was observed that the fluorescent intensity of DOX in HeLa cells increased intensely after NIR irradiation. It was speculated the thermoresponsive polymer valve remained in a closed state to hinder the release of DOX without NIR irradiation, which might induce the fluorescent quenching of loaded DOX via fluorescence resonance energy transfer effect due to the existing rNGO.<sup>29, 53, 54</sup> Additionally, under NIR irradiation, the heats induced by rNGO not only opened the thermoresponsive polymer valve but also promoted the diffusion of adsorbed DOX, retrieving the intense fluorescence of DOX for real-time monitor of the release process.<sup>55</sup> Moreover, the spherical and cracked cells under NIR irradiation,

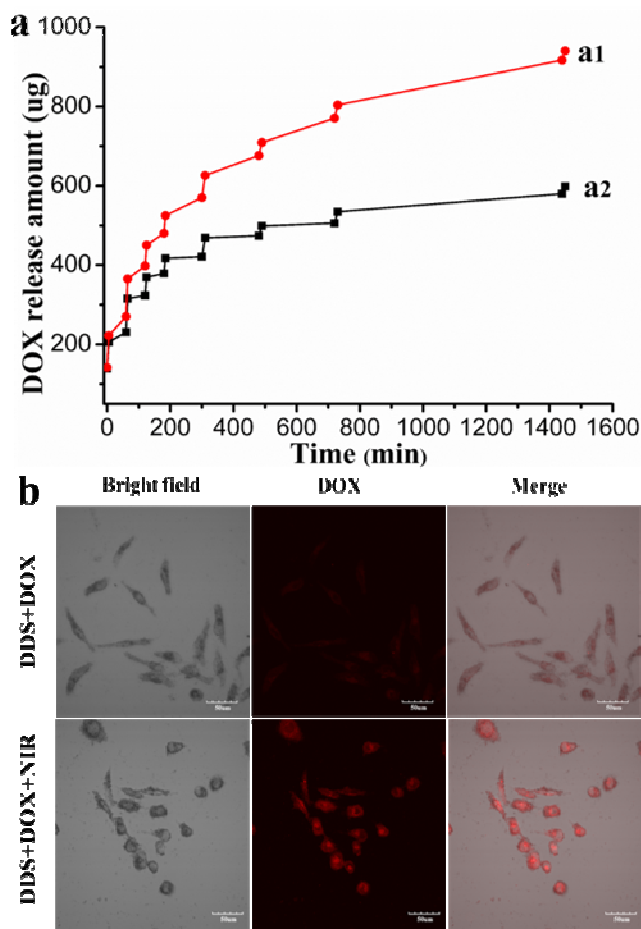


**Fig. 6** The release curve of loaded DOX in the KH<sub>2</sub>PO<sub>4</sub> buffer (pH=5) from rNGO@mSiO<sub>2</sub> (a1) or rNGO@mSiO<sub>2</sub>@pNIPAM-co-pAAm (a2) with NIR irradiation at determined time; the CLSM images of HeLa cells incubated by 60  $\mu$ g/mL rNGO@mSiO<sub>2</sub>@pNIPAM-co-pAAm (DDS) containing 12  $\mu$ g/mL DOX with or without NIR irradiation (b).

which reflected potential apoptotic HeLa cells, further hinting the efficient NIR controlled treatments for HeLa cells.

In order to probe the potential in vivo application of rNGO@mSiO<sub>2</sub>@pNIPAM-co-pAAm in the future, a chunk of fresh meat was encompassed around centrifugation tube which contained KH<sub>2</sub>PO<sub>4</sub> solution of DOX loaded rNGO@mSiO<sub>2</sub>@pNIPAM-co-pAAm (pH=5) to simulate in vivo condition and the heating and drug release behaviour were investigated under NIR irradiation. Through the experiment, it was found the thickness of meat would affect the heating efficacy to the most extent. Three thickness (1.5, 3 and 5 mm) of meat was conducted in parallel and the temperature could reach the demand of hyperthermia ( $T > 42$  °C) for all cases within 5 min. Then the drug release behaviour was recorded in the case of 3 mm thickness meat. Without NIR irradiation, the release of DOX was quite a little, however, a burst release happened once irradiated, all of which identified the feasibility of in vivo application of rNGO@mSiO<sub>2</sub>@pNIPAM-co-pAAm in the future (Fig. S9†).

#### The applications of the rNGO@mSiO<sub>2</sub>@pNIPAM-co-pAAm in cancer therapy

Before further application in HeLa cells, the low toxicity of rNGO@mSiO<sub>2</sub>@pNIPAM-co-pAAm was evaluated with the cell

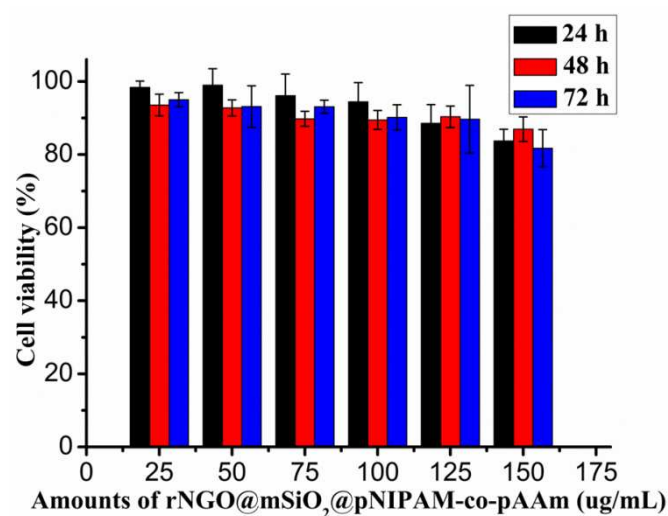


**Fig. 7** The viability of HeLa cells incubated with rNGO@mSiO<sub>2</sub>@pNIPAM-co-pAAm (25-150 µg/mL) for different time.

counting kit-8 (CCK-8) assay. Different amounts of the rNGO@mSiO<sub>2</sub>@pNIPAM-co-pAAm (25-150 µg/mL) were incubated with HeLa cells for 24, 48 and 72 h. In Fig. 7, it was observed that the cell viability kept above 80% even with the concentration of 150 µg/mL for 72 h, which was acceptable for intracellular drug delivery. Compared with the pristine rNGO@mSiO<sub>2</sub>, the grafted polymer would enhance the dispersibility and stability of this material, which would be stable in the PBS buffer for more than one week and favourable for intracellular applications. We assumed the excellent dispersibility and stability were because the zeta potential of rNGO@mSiO<sub>2</sub> increased from -52.1 mV to -6.40 mV (Fig. S10†) after the successful grafting of the thermoresponsive polymer (rNGO@mSiO<sub>2</sub>@pNIPAM-co-pAAm) and the nearly electro neutral nanocarriers can not mutually attract enough ions through electrostatic effect in the PBS buffer to cause aggregates but form the inter-molecule hydrogen bonds with water molecules and steric hindrance between the stretched polymer chains to maintain excellent dispersibility and stability.

The DOX loaded rNGO@mSiO<sub>2</sub>@pNIPAM-co-pAAm (rNGO@mSiO<sub>2</sub>@pNIPAM-co-pAAm/DOX) was applied to treat HeLa cells with controlled chemo-photothermal synergistic therapy under the remote manipulation by NIR irradiation (Fig. 8a). At first, the photothermal treating efficacy of the rNGO@mSiO<sub>2</sub>@pNIPAM-co-pAAm was investigated. Under the exposure of NIR irradiation for 10 min, only 64.32% HeLa cells could survive when treated with 60 µg/mL rNGO@mSiO<sub>2</sub>@pNIPAM-co-pAAm, compared with 96.13% viable cells without the involvement of the rNGO@mSiO<sub>2</sub>@pNIPAM-co-pAAm, which implied the efficient photothermal therapy and non-phototoxicity of NIR alone (Fig. 8b red and brown bar). Yet, due to insufficient efficiency in generating heats during NIR irradiation, lower concentration of rNGO@mSiO<sub>2</sub>@pNIPAM-co-pAAm induced mild toxicity for HeLa cells during the photothermal treatment. In the following process, the chemotherapy was conducted through the incubation of HeLa cells with DOX loaded rNGO@mSiO<sub>2</sub> without thermoresponsive polymer valve where the bare rNGO@mSiO<sub>2</sub> showed negligible toxicity to cells (Fig. S11†). The therapeutic effect of rNGO@mSiO<sub>2</sub>/DOX showed a dose-dependent manner and almost 34% cells were killed when 60 µg/mL rNGO@mSiO<sub>2</sub> containing 12 µg/mL DOX was applied, revealing the relatively efficient chemotherapy effect attributed to the sustainable release of DOX (Fig. 8b blue bar).

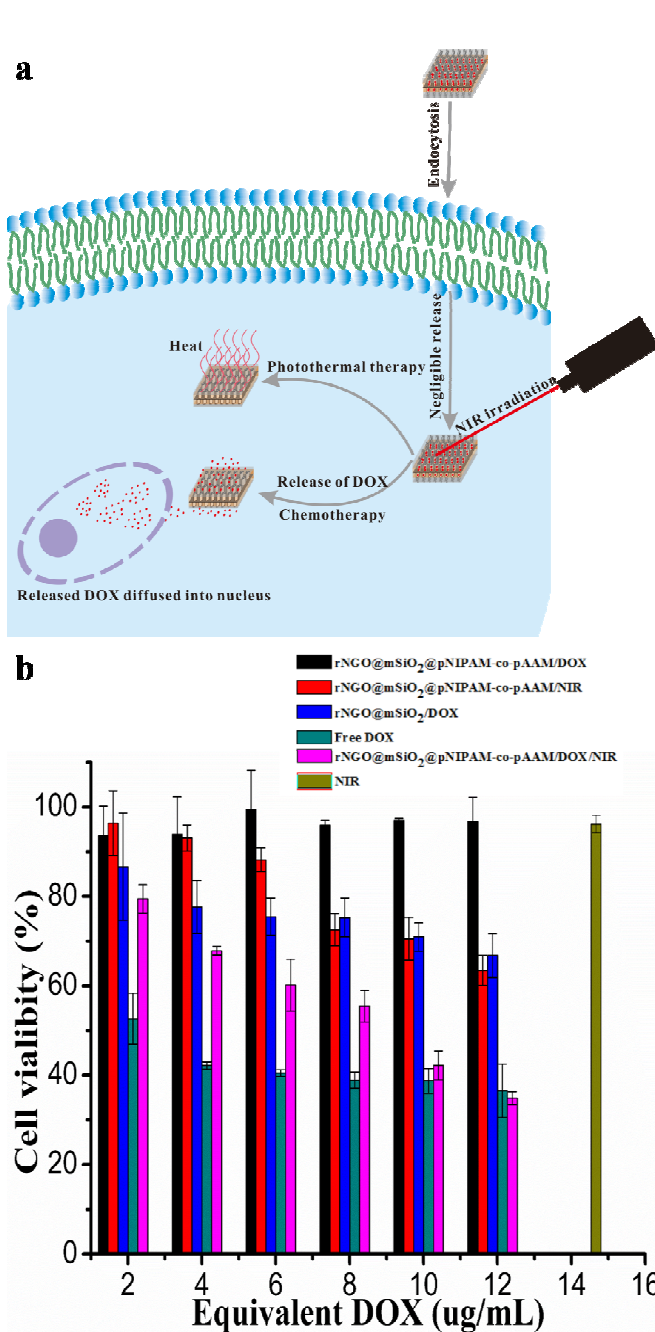


**Fig. 8** A schematic illustration of the process of intracellular controlled release of loaded DOX by NIR irradiation with the chemo-photothermal synergistic cancer therapy (a) and the viability of HeLa cells under the conditions of rNGO@mSiO<sub>2</sub>@pNIPAM-co-pAAm/DOX (black bar), rNGO@mSiO<sub>2</sub>@pNIPAM-co-pAAm/NIR (red bar), rNGO@mSiO<sub>2</sub>/DOX (blue bar), free DOX (green bar), rNGO@mSiO<sub>2</sub>@pNIPAM-co-pAAm/DOX/NIR (pink bar) and NIR (brown bar) (b).

Secondly, the synergistic anticancer efficacy of rNGO@mSiO<sub>2</sub>@pNIPAM-co-pAAm/DOX under NIR remote manipulation was profiled. By incubation with rNGO@mSiO<sub>2</sub>@pNIPAM-co-pAAm/DOX (10-60 µg/mL rNGO@mSiO<sub>2</sub>@pNIPAM-co-pAAm containing 2-12 µg/mL loaded DOX), viability of HeLa cells with or without NIR irradiation was measured. Shown in Fig. 8b, rNGO@mSiO<sub>2</sub>@pNIPAM-co-pAAm/DOX without NIR irradiation exhibited negligible toxicity to

HeLa cells (black bar), while the killing efficiency increased greatly after NIR irradiation (rNGO@mSiO<sub>2</sub>@pNIPAM-co-pAAm/DOX/NIR) was performed (Fig. 8b pink bar). Since the rNGO@mSiO<sub>2</sub>@pNIPAM-co-pAAm/DOX was taken up by HeLa cells via endocytosis during incubation, normally the acidic and high-level GSH amount atmosphere would facilitate the release of DOX because of the protonation of DOX and disruption of  $\pi$ - $\pi$  stacking effect between DOX and rNGO, inducing the cell apoptosis as rNGO@mSiO<sub>2</sub>/DOX did (Fig. 8b blue bar).<sup>55, 56</sup> Thus, the negligible cytotoxicity for rNGO@mSiO<sub>2</sub>@pNIPAM-co-pAAm/DOX without NIR irradiation confirmed the utility of the thermoresponsive polymer valve in blocking the diffusion of DOX, matching well the results of a recent work published by Yang et al.<sup>48</sup> rNGO in the rNGO@mSiO<sub>2</sub>@pNIPAM-co-pAAm were assigned for the generation of heats during NIR irradiation, which was utilized to open the thermoresponsive polymer valve, promote the diffusion of DOX and present the photothermal treatment. As discussed above, the heats generated by rNGO were positively correlated to the concentration of rNGO@mSiO<sub>2</sub>@pNIPAM-co-pAAm, so at relatively low concentration, such as 30  $\mu$ g/mL, the treating efficacy of rNGO@mSiO<sub>2</sub>@pNIPAM-co-pAAm/DOX/NIR was moderate. On one hand, because of the limited amount of ingested rNGO, the heats conversion via rNGO@mSiO<sub>2</sub>@pNIPAM-co-pAAm was insufficient to cause the complete collapse of polymer brushes and promote the release of DOX, resulting in the inferior effect of chemotherapy. On the other hand, as indicated by Fig. 8b, the photothermal effect was not obvious at the concentration below 30  $\mu$ g/mL, which meant the effect of photothermal therapy would not embody efficiently in this case. As a result, the maximum of treating efficacy of rNGO@mSiO<sub>2</sub>@pNIPAM-co-pAAm/DOX/NIR was obtained with 60  $\mu$ g/mL rNGO@mSiO<sub>2</sub>@pNIPAM-co-pAAm containing 12  $\mu$ g/mL DOX. When compared with free DOX, the rNGO@mSiO<sub>2</sub>@pNIPAM-co-pAAm/DOX/NIR (below 60  $\mu$ g/mL) exhibited a less effective performance in killing HeLa cells due to the gradual diffusion of loaded DOX rather than the direct administration with free DOX. However, the therapeutic effect of rNGO@mSiO<sub>2</sub>@pNIPAM-co-pAAm/DOX/NIR went close with free DOX as the concentration of rNGO@mSiO<sub>2</sub>@pNIPAM-co-pAAm increased and was even better than that of free DOX as 60  $\mu$ g/mL rNGO@mSiO<sub>2</sub>@pNIPAM-co-pAAm/DOX was applied, which might be attributed to the chemo-photothermal synergistic therapy. Moreover, it was obvious to find out the therapeutic effect of rNGO@mSiO<sub>2</sub>@pNIPAM-co-pAAm/NIR (photothermal therapy) or rNGO@mSiO<sub>2</sub>/DOX (chemotherapy) alone fell behind rNGO@mSiO<sub>2</sub>@pNIPAM-co-pAAm/DOX/NIR (synergistic therapy) at every determined amount, further demonstrating the high potency of chemo-photothermal synergistic therapy in dealing with the cancer.

As another proof, the feasibility of NIR irradiation as a stimulus for controlled chemo-photothermal synergistic cancer therapy was also evaluated via the observation of HeLa cells treated with rNGO@mSiO<sub>2</sub>@pNIPAM-co-pAAm/DOX, rNGO@mSiO<sub>2</sub>@pNIPAM-co-pAAm/NIR, rNGO@mSiO<sub>2</sub>/DOX and rNGO@mSiO<sub>2</sub>@pNIPAM-co-pAAm/DOX/NIR by an Olympus microscopy, where the dead cells were stained with Trypan blue. It was observed that HeLa cells were efficiently killed only under the treatment with rNGO@mSiO<sub>2</sub>@pNIPAM-co-pAAm/DOX/NIR, followed by the moderate and negligible killing efficacy for the case of rNGO@mSiO<sub>2</sub>@pNIPAM-co-pAAm/NIR, rNGO@mSiO<sub>2</sub>/DOX and rNGO@mSiO<sub>2</sub>@pNIPAM-co-pAAm/DOX, respectively, which were consistent with the results from cell viability assay (Fig. 9a-d). Moreover, NIR irradiation was an external stimulus in the remote controlled drug release, and the confined beam of NIR laser could also provide site-targeted treatments, which might reduce the severe

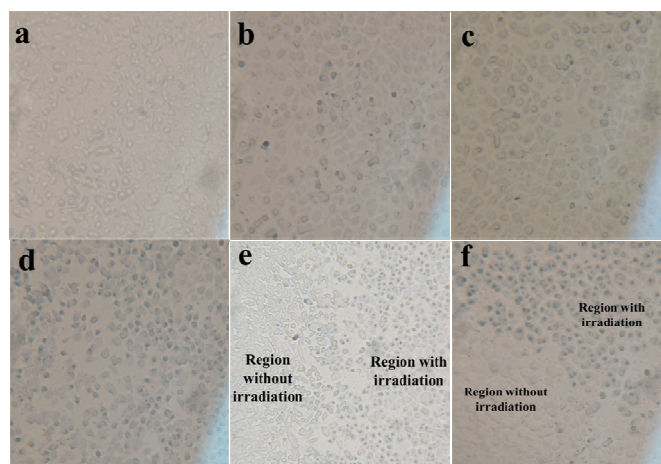


**Fig. 9** The images of HeLa cells stained with Trypan blue under the treatments of rNGO@mSiO<sub>2</sub>@pNIPAM-co-pAAm/DOX (a), rNGO@mSiO<sub>2</sub>@pNIPAM-co-pAAm/NIR (b), rNGO@mSiO<sub>2</sub>/DOX (c) and rNGO@mSiO<sub>2</sub>@pNIPAM-co-pAAm/DOX/NIR (d); The images of HeLa cells stained with Trypan blue under NIR site-targeted treatment (e, f).

damages of normal cells during administration. To test the hypothesis, rNGO@mSiO<sub>2</sub>@pNIPAM-co-pAAm/DOX was employed to treat with HeLa cells in the culture plate for 12 h, where only one part of region was exposed under NIR irradiation. By observation with an Olympus microscopy, HeLa cells were only efficiently killed in the region with NIR irradiation, and the surrounding cells survived during the selective treatments (Fig. 9e and 9f). Thus, the rNGO@mSiO<sub>2</sub>@pNIPAM-co-pAAm/DOX coupled with NIR irradiation implied potentials for the site-targeted in vivo treatments in the future.

## Conclusion

In summary, a novel nanocarrier for spatiotemporally NIR controlled chemo-photothermal synergistic cancer therapy was successfully synthesized, based on the sol-gel assembly of the mesoporous silica shell to coat the rNGO and polymerization of the thermoresponsive pNIPAM-co-pAAm valve with ATRP strategy onto the outlet of the silica pore channels. The rNGO were efficient in converting NIR irradiation into heats so as to “open” the thermoresponsive polymer valve outside the silica pore channels and promote the diffusion of loaded DOX as well as present the photothermal treatment for cancer cells. The nanocarrier demonstrated to be low toxicity with controlled and site-targeted anti-cancer treatments for HeLa cells. Moreover, the synergistic treatments of chemo-photothermal therapy endowed the nanocarrier with the enhanced therapeutic efficacy. The efficient manipulation of the release of loaded DOX from rNGO@mSiO<sub>2</sub>@pNIPAM-co-pAAm via NIR irradiation also implied potential applications of the nanocarrier in intracellular delivery of different agents. Furthermore, it might also broaden sights in fabrication of remote controlled intracellular delivery nanovehicles.

## Acknowledgements

This work was supported by the China State Key Basic Research Program Grant (2013CB911202, 2012CB910101, 2012CB910604), the Creative Research Group Project of NSFC (21321064), the National Natural Science Foundation of China (21235006, 81161120540), National Key Special Program on Infection diseases (2012ZX10002009-011), Analytical Method Innovation Program of MOST (2012IM030900).

## Notes and references

- <sup>a</sup> CAS Key Laboratory of Separation Sciences for Analytical Chemistry, National Chromatographic R&A Center, Dalian Institute of Chemical Physics, Chinese Academy of Sciences (CAS), Dalian 116023, China; E-mail: hanfazou@dicp.ac.cn.
- <sup>b</sup> Shanghai Key Laboratory of Functional Materials Chemistry, East China University of Science and Technology, Shanghai 200237, China. E-mail: weibingzhang@ecust.edu.cn
- Electronic Supplementary Information (ESI) available: [details of any supplementary information available should be included here]. See DOI: 10.1039/b000000x/
- S. Zhang, Z. Chu, C. Yin, C. Zhang, G. Lin and Q. Li, *J. Am. Chem. Soc.*, 2013, **135**, 5709-5716.
  - M. Li, P. Shi, C. Xu, J. Ren and X. Qu, *Chem. Sci.*, 2013, **4**, 2536.
  - W. Cao, Y. Li, Y. Yi, S. Ji, L. Zeng, Z. Sun and H. Xu, *Chem. Sci.*, 2012, **3**, 3403-3408.
  - J. H. Lee, K. J. Chen, S. H. Noh, M. A. Garcia, H. Wang, W. Y. Lin, H. Jeong, B. J. Kong, D. B. Stout, J. Cheon and H. R. Tseng, *Angew. Chemie., Int. Ed.*, 2013, **52**, 4384-4388.
  - Q. An, J. Brinkmann, J. Huskens, S. Krabbenborg, J. de Boer and P. Jonkhøj, *Angew. Chemie., Int. Ed.*, 2012, **51**, 12233-12237.
  - K. Khaletskaya, J. Reboul, M. Meilikhov, M. Nakahama, S. Diring, M. Tsujimoto, S. Isoda, F. Kim, K. Kamei, R. A. Fischer, S. Kitagawa and S. Furukawa, *J. Am. Chem. Soc.*, 2013, **135**, 10998-11005.
  - L. Wen, Q. Liu, J. Ma, Y. Tian, C. Li, Z. Bo and L. Jiang, *Adv. Mater.*, 2012, **24**, 6193-6198.
  - D. He, X. He, K. Wang, J. Cao and Y. Zhao, *Adv. Funct. Mater.*, 2012, **22**, 4704-4710.
  - J. Lai, X. Mu, Y. Xu, X. Wu, C. Wu, C. Li, J. Chen and Y. Zhao, *Chem. Commun.*, 2010, **46**, 7370-7372.
  - X. Mei, S. Yang, D. Chen, N. Li, H. Li, Q. Xu, J. Ge and J. Lu, *Chem. Commun.*, 2012, **48**, 10010-10012.
  - N. Li, Z. Yu, W. Pan, Y. Han, T. Zhang and B. Tang, *Adv. Funct. Mater.*, 2013, **23**, 2255-2262.
  - J. Cao, S. Huang, Y. Chen, S. Li, X. Li, D. Deng, Z. Qian, L. Tang and Y. Gu, *Biomaterials.*, 2013, **34**, 6272-6283.
  - L. Sun, X. Ma, C. M. Dong, B. Zhu and X. Zhu, *Biomacromolecules.*, 2012, **13**, 3581-3591.
  - J. He, Z. Wei, L. Wang, Z. Tomova, T. Babu, C. Wang, X. Han, J. T. Fourkas and Z. Nie, *Angew. Chemie., Int. Ed.*, 2013, **52**, 2463-2468.
  - J. He, P. Zhang, T. Babu, Y. Liu, J. Gong and Z. Nie, *Chem. Commun.*, 2013, **49**, 576-578.
  - K. Dong, Z. Liu, Z. Li, J. Ren and X. Qu, *Adv. Mater.*, 2013, **25**, 4452-4458.
  - A. F. Bagley, S. Hill, G. S. Rogers and S. N. Bhatia, *ACS Nano.*, 2013, **7**, 8089-8097.
  - Q. Xiao, X. Zheng, W. Bu, W. Ge, S. Zhang, F. Chen, H. Xing, Q. Ren, W. Fan, K. Zhao, Y. Hua and J. Shi, *J. Am. Chem. Soc.*, 2013, **135**, 13041-13048.
  - C. M. Hessel, V. P. Pattani, M. Rasch, M. G. Panthani, B. Koo, J. W. Tunnell and B. A. Korgel, *Nano letters.*, 2011, **11**, 2560-2566.
  - G. T. Spence, G. V. Hartland and B. D. Smith, *Chem. Sci.*, 2013, **4**, 4240.
  - C. Wang, H. Xu, C. Liang, Y. Liu, Z. Li, G. Yang, L. Cheng, Y. Li and Z. Liu, *ACS Nano.*, 2013, **7**, 6782-6795.
  - Z. Jiang, B. Dong, B. Chen, J. Wang, L. Xu, S. Zhang and H. Song, *Small.*, 2013, **9**, 604-612.
  - H. W. Yang, Y. J. Lu, K. J. Lin, S. C. Hsu, C. Y. Huang, S. H. She, H. L. Liu, C. W. Lin, M. C. Xiao, S. P. Wey, P. Y. Chen, T. C. Yen, K. C. Wei and C. C. Ma, *Biomaterials.*, 2013, **34**, 7204-7214.
  - W. Li, F. Wang, S. Feng, J. Wang, Z. Sun, B. Li, Y. Li, J. Yang, A. A. Elzatahry, Y. Xia and D. Zhao, *J. Am. Chem. Soc.*, 2013, **135**, 18300-18303.
  - G. Lu, H. Li, C. Liusman, Z. Yin, S. Wu and H. Zhang, *Chem. Sci.*, 2011, **2**, 1817-1821.
  - Z. Ren, E. Kim, S. W. Pattinson, K. S. Subrahmanyam, C. N. R. Rao, A. K. Cheetham and D. Eder, *Chem. Sci.*, 2012, **3**, 209-216.
  - M.-C. Wu, A. R. Deokar, J.-H. Liao, P.-Y. Shih and Y.-C. Ling, *ACS Nano.*, 2013, **7**, 1281-1290.
  - X. Shi, H. Gong, Y. Li, C. Wang, L. Cheng and Z. Liu, *Biomaterials.*, 2013, **34**, 4786-4793.
  - W. Miao, G. Shim, S. Lee, S. Lee, Y. S. Choe and Y. K. Oh, *Biomaterials.*, 2013, **34**, 3402-3410.
  - H. J. Yoon, T. H. Kim, Z. Zhang, E. Azizi, T. M. Pham, C. Paoletti, J. Lin, N. Ramnath, M. S. Wicha, D. F. Hayes, D. M. Simeone and S. Nagrath, *Nat. Nano.*, 2013, **8**, 735-741.
  - W. Li, J. Wang, J. Ren and X. Qu, *Angew. Chemie., Int. Ed.*, 2013, **52**, 6726-6730.
  - W. Wei, K. Qu, J. Ren and X. Qu, *Chem. Sci.*, 2011, **2**, 2050-2056.
  - C. Cheng, S. Li, S. Nie, W. Zhao, H. Yang, S. Sun and C. Zhao, *Biomacromolecules.*, 2012, **13**, 4236-4246.
  - P. Yin, M. Zhao and C. Deng, *Nanoscale.*, 2012, **4**, 6948-6950.
  - Z.-M. Wang, W. Wang, N. Coombs, N. Soheilnia and G. A. Ozin, *ACS Nano*, 2010, **4**, 7437-7450.
  - U. Patil, A. Fihri, A.-H. Emwas and V. Polshettiwar, *Chem. Sci.*, 2012, **3**, 2224-2229.
  - P. Yin, Y. Wang, Y. Li, C. Deng, X. Zhang and P. Yang, *Proteomics.*, 2012, **12**, 2784-2791.
  - Z. S. Wu, Y. Sun, Y. Z. Tan, S. Yang, X. Feng and K. Mullen, *J. Am. Chem. Soc.*, 2012, **134**, 19532-19535.
  - S. Yang, X. Feng and K. Mullen, *Adv. Mater.*, 2011, **23**, 3575-3579.
  - Y. Wang, K. Y. Wang, J. F. Zhao, X. G. Liu, J. Bu, X. Y. Yan and R. Q. Huang, *J. Am. Chem. Soc.*, 2013, **135**, 4799-4804.
  - A. C. Rotzetter, C. M. Schumacher, S. B. Bubenhofer, R. N. Grass, L. C. Gerber, M. Zeltner and W. J. Stark, *Adv. Mater.*, 2012, **24**, 5352-5356.
  - J. Liu, S. Bai, Q. Jin, C. Li and Q. Yang, *Chem. Sci.*, 2012, **3**, 3398-3402.
  - A. Baeza, E. Guisasaola, E. Ruiz-Hernández and M. Vallet-Regí, *Chem. Mater.*, 2012, **24**, 517-524.
  - M. Szuwarzyński, L. Zaraska, G. D. Sulka and S. Zapotoczny, *Chem. Mater.*, 2013, **25**, 514-520.
  - H. Yang, K. Paek and B. J. Kim, *Nanoscale.*, 2013, **5**, 5720-5724.
  - N. Singh, A. Karambelkar, L. Gu, K. Lin, J. S. Miller, C. S. Chen, M. J. Sailor and S. N. Bhatia, *J. Am. Chem. Soc.*, 2011, **133**, 19582-19585.
  - Z. Zhang, S. Maji, A. B. d. F. Antunes, R. De Rycke, Q. Zhang, R. Hoogenboom and B. G. De Geest, *Chem. Mater.*, 2013, **25**, 4297-4303.

48. J. P. Yang, D. K. Shen, L. Zhou, W. Li, X. M. Xiao, C. Yao, R. Wang, A. M. El-Toni, F. Zhang, D. Y. Zhao, *Chem. Mater.*, 2013, **25**, 3030-3037.
49. L. E. Strong, S. N. Dahotre, J. L. West, *J Control Release.*, 2014, **178**, 63-68.
50. M. S. Yavuz, Y. Cheng, J. Chen, C. M. Cobley, Q. Zhang, M. Rycenga, J. Xie, C. Kim, K. H. Song, A. G. Schwartz, L. V. Wang and Y. Xia, *Nat. Mater.*, 2009, **8**, 935-939.
51. X. Fan, W. Peng, Y. Li, X. Li, S. Wang, G. Zhang and F. Zhang, *Adv Mater.*, 2008, **20**, 4490-4493.
52. Y. Liu, K. Ai, J. Liu, M. Deng, Y. He and L. Lu, *Adv Mater.*, 2013, **25**, 1353-1359.
53. H. L. Zhang, X. L. Wei, Y. Zang, J. Y. Cao, S. Liu, X. P. He, Q. Chen, Y. T. Long, J. Li, G. R. Chen and K. Chen, *Adv Mater.*, 2013, **25**, 4097-4101.
54. J. Tang, B. Kong, H. Wu, M. Xu, Y. Wang, Y. Wang, D. Zhao and G. Zheng, *Adv Mater.*, 2013, **25**, 6569-6574.
55. H. Kim, D. Lee, J. Kim, T.-i. Kim and W. J. Kim, *ACS Nano.*, 2013, **7**, 6735-6746.
56. U. Dembereldorj, M. Kim, S. Kim, E.-O. Ganbold, S. Y. Lee and S.-W. Joo, *J. Mater. Chem.*, 2012, **22**, 23845.

25